Supporting Information for

Harnessing a Germ-Free Mouse Gut Bioreactor for Directed Evolution of Probiotics to Combat Non-Alcoholic Fatty Liver Disease

Zhe Han[1, 2, #], Zheng Sun[3, # ✉], Xinlei Liu[1, 2], Dongyu Zhen[1, 2], Quan Guo[1, 2], Leijie Zheng[1, 2], Shuaiming Jiang[1, 2], Zeng Zhang[1, 2], Siyuan Shen[1, 2], Jiachao Zhang[1, 2 ✉]

[1]School of Food Science and Engineering, Key Laboratory of Food Nutrition and Functional Food of Hainan Province, Hainan University, Haikou, Hainan 570228, China.
[2]Collaborative Innovation Center of One Health, Hainan University, Haikou, Hainan 570228, China.
[3]Channing Division of Network Medicine, Department of Medicine, Brigham and Women's Hospital and Harvard Medical School, Boston, MA 02115, USA.

[#]These authors contributed equally: Zhe Han, Zheng Sun.

Corresponding authors: Zheng Sun, Jiachao Zhang
✉e-mail: spzsu@channing.harvard.edu; jiachao@hainanu.edu.cn

This PDF file includes:
Supplementary Figures 1 to 8

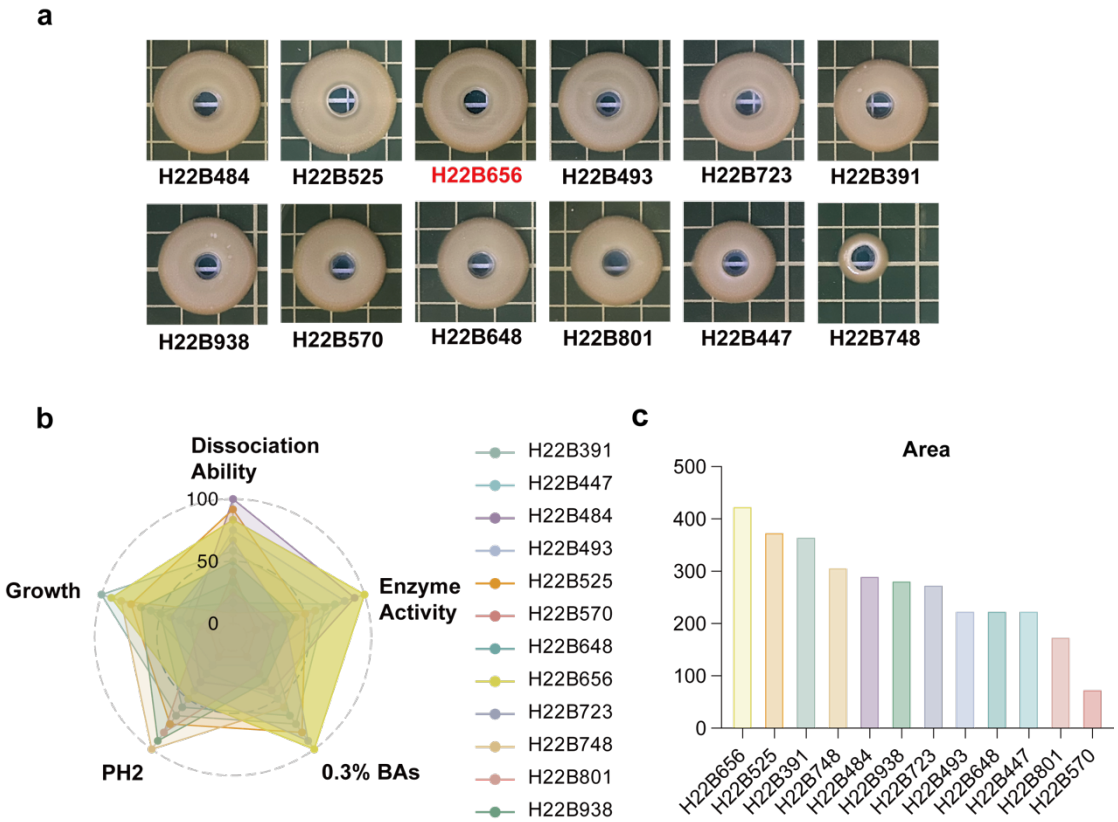

Supplementary Fig. 1 Phenotypic Profiling and High-Confidence SNV Detection. (a) Calcium solubilization by each strain after 48 h of anaerobic incubation in bile-salt medium supplemented with sodium thioglycolate and $CaCl_2$ (n = 3). **(b, c)** Composite scores for each strain, calculated by converting individual phenotypic metrics to percentile ranks and summing them. **(d)** Application of InStrain and BCftools pipelines to the W5S9 sample, jointly identifying 282 high-confidence SNVs. Source data are provided as a Source Data file.

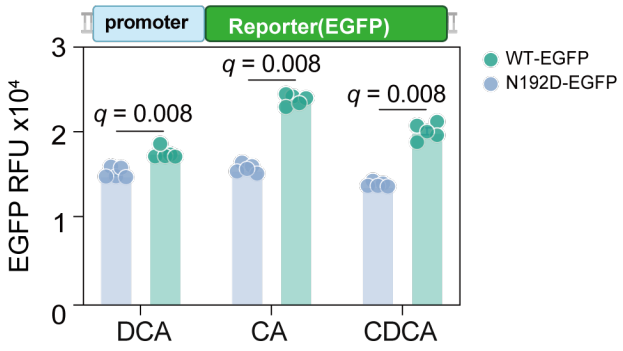

Supplementary Fig. 2 N192D substitution enhances *mdr* translation under bile acid stress in *E. coli*. EGFP fluorescence intensities in *E. coli* BL21(DE3) cells harboring reporter plasmids encoding WT-EGFP or N192D-EGFP following treatment with DCA, CA, and CDCA. Data are presented as mean ± SEM ($n = 5$). Differences between groups were analyzed using multiple Mann-Whitney tests. To correct for multiple comparisons, the False Discovery Rate (FDR) was controlled using the two-stage step-up method (Benjamini, Krieger, and Yekutieli), with a desired FDR (Q) set at 1.00%. Dots represent individual data. Source data are provided as a Source Data file.

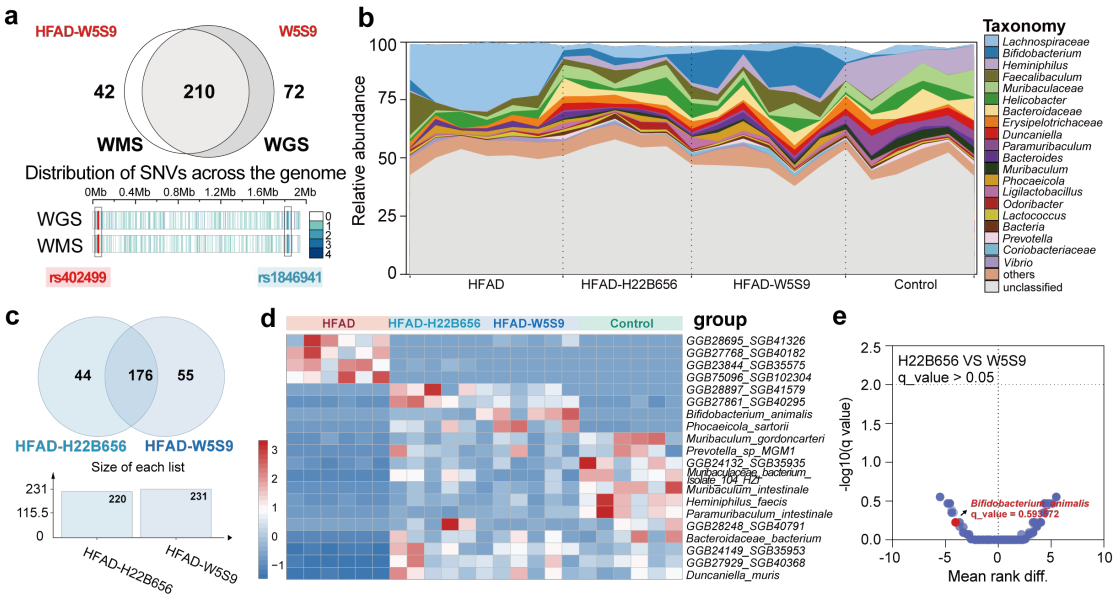

Supplementary Fig. 3 Effects of *B. animalis* subsp. *lactis* H22B656 and *B. animalis* subsp. *lactis* W5S9 interventions on intestinal microbiota composition. (a) The Venn diagram depicts the overlap of SNVs called by whole-metagenome shotgun (WMS) sequencing in the HFAD-W5S9 group and by whole-genome sequencing (WGS) of the adapted W5S9 strain. Two key SNVs were annotated in the HFAD-W5S9 samples but were not detected in the HFAD-H22B656 group, indicating that no cross-contamination occurred between the gavaged strains. **(b)** Stacked area chart showing the relative abundance of bacterial taxa at the family and genus levels across the HFAD, HFAD-H22B656, HFAD-W5S9, and Control group. **(c)** Venn diagram illustrating the number of shared and unique species between the HFAD-H22B656 and HFAD-W5S9 groups. **(d)** Heatmap showing the relative abundance of specific bacterial species across all groups. The color scale represents the normalized abundance (Z-score), with red indicating higher abundance and blue indicating lower abundance. **(e)** Volcano plot comparing the differential abundance of gut microbiota between the HFAD-H22B656 and HFAD-W5S9 groups. Differences between groups (e.g., H22B656 vs. W5S9) were analyzed using multiple Mann-Whitney tests. To correct for multiple comparisons, the False Discovery Rate (FDR) was controlled using the two-stage step-up method (Benjamini, Krieger, and Yekutieli), with a desired FDR (Q) set at 1.00%. The red dot highlights *Bifidobacterium animalis*, indicating no significant difference (q-value > 0.05) between the two probiotic treatments. Data are presented as $n = 6$ mice per group. Source data are provided as a Source Data file.

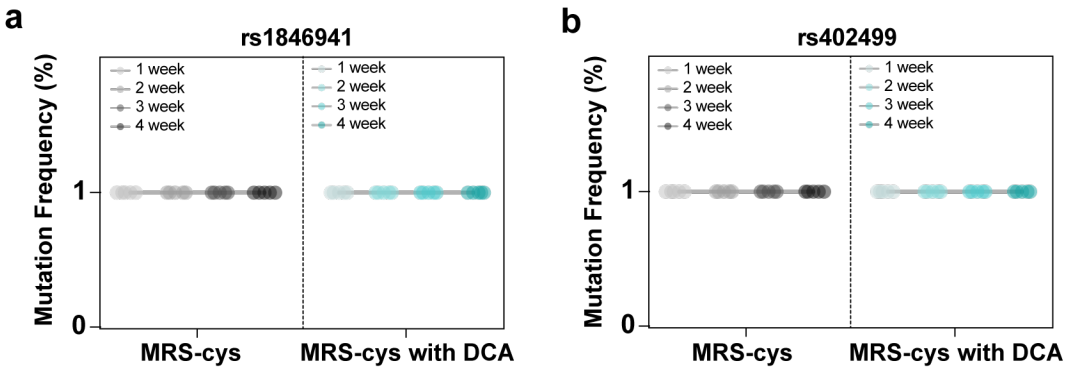

Supplementary Fig. 4 Genetic Stability of rs1846941 and rs402499. Mutation frequency of the key SNVs (**a**) rs1846941 and (**b**) rs402499 in the adapted strain over a 4-week period under continuous passage conditions. The mutation frequency was assessed in MRS-cys medium (control) and in MRS-cys medium supplemented with 0.3% deoxycholic acid (DCA) as the bile salt stress (n = 5 per week). Source data are provided as a Source Data file.

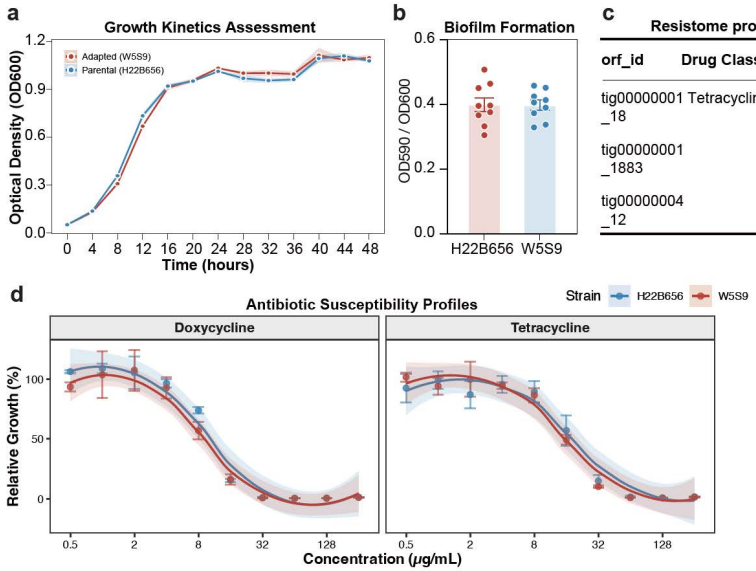

Supplementary Fig. 5 Safety evaluation of the parental *B. animalis* subsp. *lactis* H22B656 and the adapted *B. animalis* subsp. *lactis* W5S9. (**a**) Growth curves over 48 h showing the growth kinetics of the two strains. Data are presented as mean ± SD. Differences between strains at each time point were analyzed using multiple unpaired t-tests. To correct for multiple comparisons, the False Discovery Rate (FDR) was controlled using the two-stage step-up method (Benjamini, Krieger, and Yekutieli), with a desired FDR (Q) set at 1.00%. (**b**) Crystal-violet biofilm formation assay after 12 h of anaerobic incubation; biofilm biomass is expressed as OD590/OD600. Data are presented as mean ± SEM. Statistical significance was determined using an unpaired two-tailed Student's t-test. (**c**) Resistome profile based on annotation with the Resistance Gene Identifier against the CARD database; only hits with >95% amino-acid identity to reference sequences are shown. orf_id, open reading frame identifier; Identity (%), percentage amino-acid identity to the reference gene. (**d**) Dose–response growth-inhibition curves of the two strains in the presence of doxycycline and tetracycline. Data are presented as mean ± SD. Statistical analysis was performed using multiple unpaired t-tests with FDR correction (Q = 1.00%), as described in (**a**). Data represent n = 3 independent biological replicates per group. Source data are provided as a Source Data file.

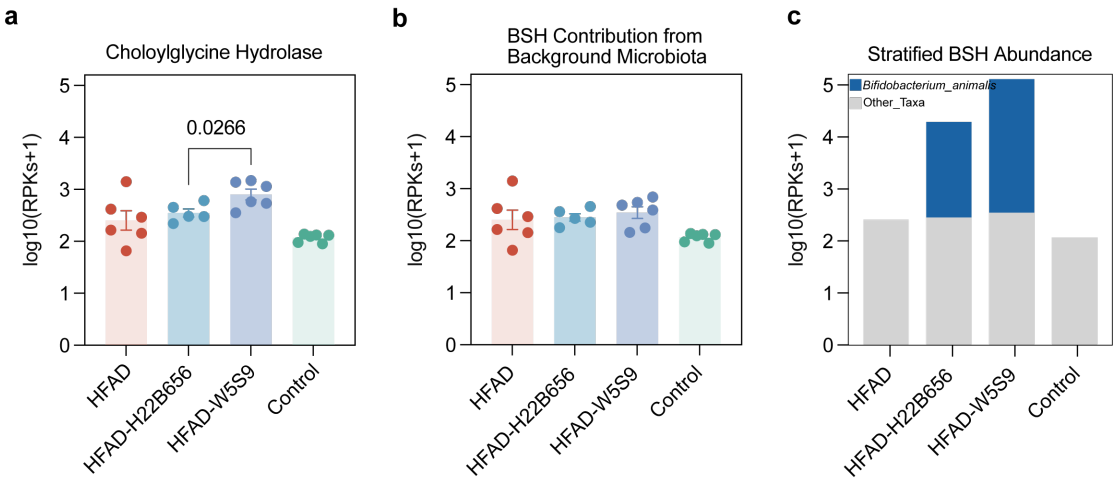

Supplementary Fig. 6. Metagenomic quantification and source attribution of bile salt hydrolase genes. (**a**) Total abundance of *cbh*-encoding genes (EC 3.5.1.24) in the gut microbiome across groups. Data are expressed as log10-transformed Reads Per Kilobase (RPKs). Data are presented as mean ± SEM. Statistical significance was determined using an unpaired two-tailed Student's t-test. (**b**) Abundance of *cbh* genes attributed exclusively to the resident background microbiota (excluding the administered *Bifidobacterium animalis*). Data are presented as mean ± SEM. Statistical significance was determined using an unpaired two-tailed Student's t-test. (**c**) Stratified analysis of BSH sources. The stacked bar chart illustrates that the elevated BSH capacity in the HFAD-W5S9 group is primarily driven by the direct contribution of *Bifidobacterium animalis*, while the contribution from other taxa remains comparable to the control and HFAD groups. Data represent $n = 6$ biological replicates per group. Source data are provided as a Source Data file.

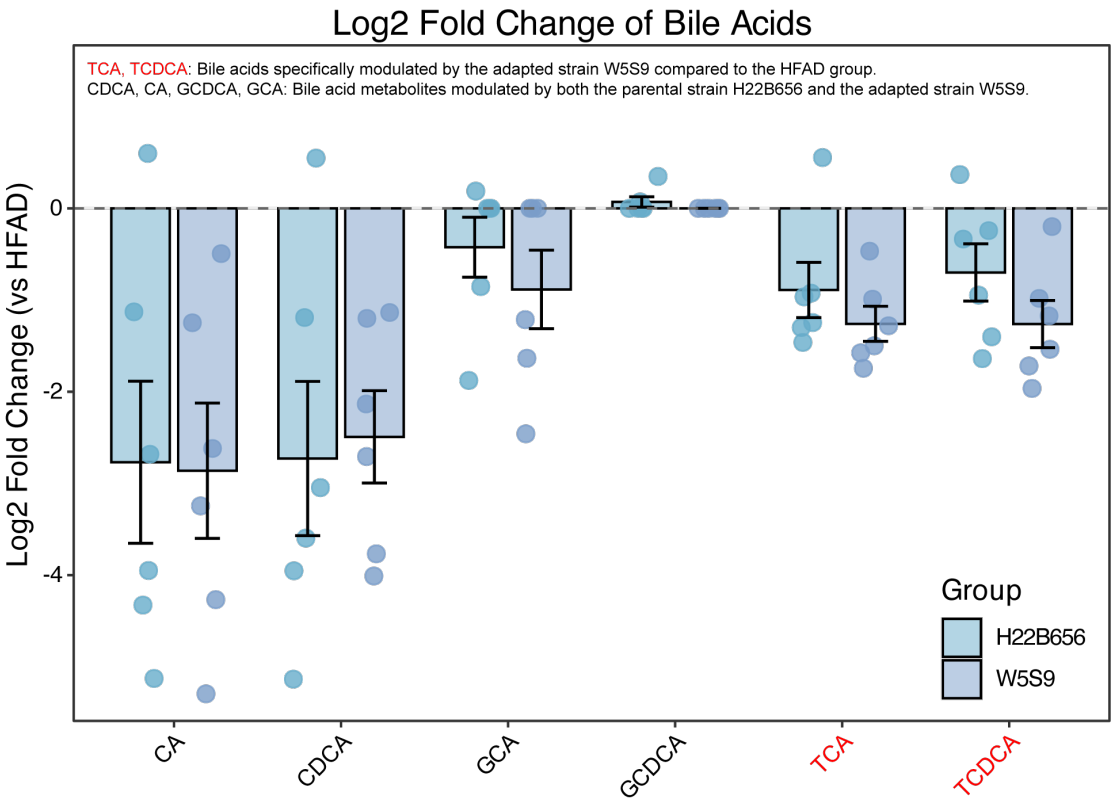

Supplementary Fig.7 Targeted bile acid metabolomics showing log2 fold change in fecal bile acid concentrations relative to the HFAD group. Bar plots represent the mean ± SEM for each bile acid metabolite, with individual dots indicating biological replicates. Differences in $\log_2$ fold change of bile acid concentrations between groups were analyzed using multiple unpaired t-tests. To correct for multiple comparisons, the False Discovery Rate (FDR) was controlled using the two-stage step-up method (Benjamini, Krieger, and Yekutieli), with a desired FDR (Q) set at 1.00%. Data represent $n = 6$ biological replicates per group. Source data are provided as a Source Data file.

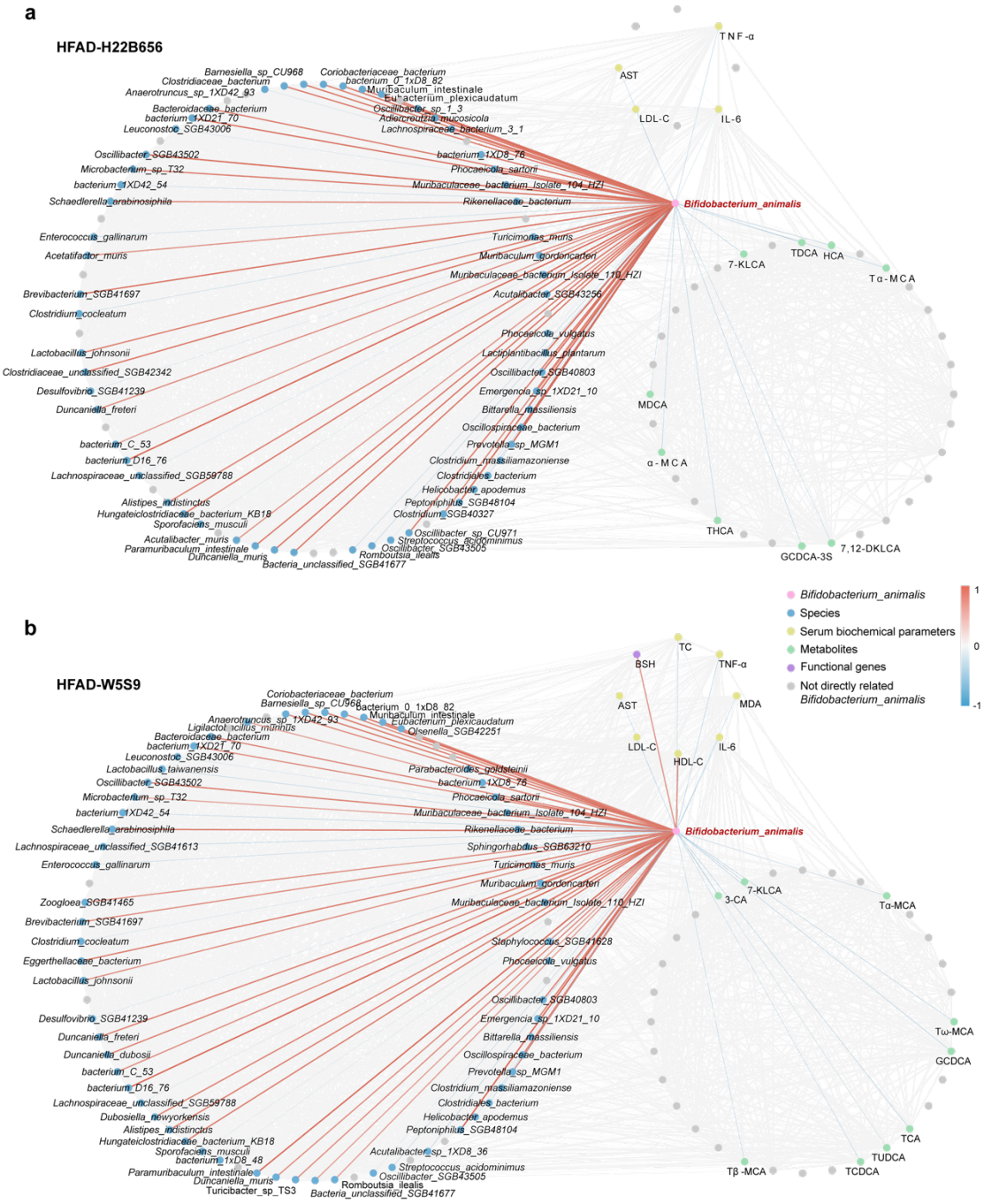

Supplementary Fig.8 Co-occurrence network analysis revealing the interaction patterns of *Bifidobacterium animalis* subsp. *lactis* with the gut ecosystem and host physiological parameters. The networks illustrate the specific correlations between *B. animalis* subsp. *lactis* and gut microbiota species, serum biochemical indices, and metabolites in the **(a)** HFAD-H22B656 and **(b)** HFAD-W5S9 groups. Nodes represent microbial species, serum biochemical parameters, bile acid metabolites, and microbial functional genes. Edges indicate significant associations determined by Spearman's rank correlation analysis ($|r|>0.4$, $p<0.05$). Red edges denote positive correlations, and blue edges denote negative correlations, with edge transparency corresponding to the magnitude of the correlation coefficient. Data are derived from $n = 6$ biological replicates per group. Source data are provided as a Source Data file.